International Journal of Physics, 2013, Vol. 1, No. 2, 28-40
Available online at http://pubs.sciepub.com/ijp/1/2/2

DOI:10.12691/ijp-1-2-2

Pulsed Laser Impact on Ferrimagnetic Nanostructures

Mykola Krupa[1], Andrii Korostil[2,*]

Department of Nanostructure Physics, Institute of Magnetism NASU, Kyiv, Ukraine
*Corresponding author: amand@rambler.ru

Received December 31, 2012; Revised March 11, 2013; Accepted April 26, 2013

Abstract We have studied the mechanisms of a pulsed laser impact on the magnetization configuration in ferrimagnetic multilayered magnetic nanostructures, specifically, tunneling magnetic junctions. The mechanism of such the laser-induced impact is a complex process of laser-induced thermal demagnetization of magnetic sublattices with subsequent biasing by internal magnetic fields of different nature. Depending on an intensity of laser pulses it can be effective internal magnetic fields of laser irradiation or internal magnetic fields connected with different rates of the heat demagnetization of ferrimagnetic sublattices. It is shown that investigated ferrimagnetic nanostructure are characterized very small times of the laser-induced remagnetization, which can attain subpicosecond scales.

Keywords: *pulsed laser radiation, ferrimagnetic nanostructures, magnetization reversal*

1. Introduction

Physical limits of remagnetization speed are one of fundamental problems of magnetism physics, which has a crucial significance for creation of magnetic high-speed recording and readout systems of information [1-6]. Growth of attention to this problem is related to modern achievements of nanotechnologies, by possibilities of production of new magnetic nanostructures with predominated physical properties, and development of the short-time pulsed laser radiation [7]. The prospect of solution of this problem associates with the use of impact of short-time laser impulses on the ferrimagnetic multilayered nanostructures, specifically, tunnel magnetic junctions [8,9,10,11,12], that can lead to magnetic state variations and the remagnetization effect [13].

The laser-induced remagnetization of a ferrimagnetic nanolayer is characterized by its initial swift heating, thermal demagnetization of ferrimagnetic sublattices with different speeds and by subsequent magnetic bias, which can be caused both laser-induced electron excitations and no equilibrium transitional magnetic states of ferrimagnetic sublattices [13,14,15,16].

The laser-induced electron excitation, occurring under circularly polarized laser radiation, results in the effective internal magnetic field H_F of the inverse magneto-optical Faraday effect and the effective internal magnetic field H_{sd} of the s-d interchange interaction of the spin-polarized current (laser-injected from a magnetic nanolayers) with the lattice magnetic moment of nanolayers. The intense laser-induced thermal demagnetization of ferrimagnetic sublattices can results in the nonequilibrium transitional state with the parallel spin configuration of ferrimagnetic sublattice, which together with an interchange interaction relaxation can cause an internal magnetic field and the remagnetization effect [13].

Such the remagnetization can occurs in the specific interval of relations between the laser pulse duration and laser-induced thermal demagnetization durations of ferrimagnetic materials [16]. The remagnetization dynamics of the ferrimagnetic nanolayers essentially depends on initial states and magnetic characteristics of ferromagnetic nanolayers. Therefore, our paper is devoted to study of features of the laser-induced remagnetization of ferrimagnetic nanostructure [13,14,15].

The structure of the presented paper is as follows. In Sec. 2, we investigate by a magneto-optical pump-probe method the laser-induced dynamics of the remagnetization and tunneling magneto-resistance effect in tunneling ferrimagnetic junctions on the basis rarer- earth and transition metal TbCoFe with perpendicular magnetic anisotropy [8,9,10,11]. It is shown the role of the laser-induced thermal demagnetization in the remagnetization under effective magnetic fields related to circularly polarized pulsed laser radiation. Sec. 3, it is studied the dependence of remagnetization dynamics on temperature behavior of an effective gyromagnetic ratio and a coercive magnetic field in ferrimagnetic junctions. Mechanisms of the laser-induced thermal remagnetization in ferrimagnetic layers with perpendicular and plane magnetic anisotropy via passing the nonequilibrium transitional magnetic state with parallel sublattice magnetizations are considered [17,18,19,20,21].

2. Laser-Induced Remagnetization under Effective Internal Magnetic Fields

The effect of the laser-induced remagnetization of thin magnetic materials represents the perspective and promising approach for increasing the physical limits of magnetic recording and information processing technologies. Based on the direct optical impact by laser pulses on magnetization this approach represents the basis for the high-speed laser control of a magnetic reversal both uniform and nonuniform magnetic systems. The laser-induced magnetic transitions in the nonuniform

multi-layered magnetic junctions can also be the basis for controlling by a spin-polarized current and the TMR in the tunnel magnetic junctions. The direct laser impact on the magnetization can be realized via the interaction its circularly polarized photons with spin-polarized electrons of a magnetic medium. The Raman-like photon excitation of the electrons together with a spin-orbital interaction are accompanied by the spin-flip of spin-polarized electrons and the remagnetization [1,2]. That represents the quantum-mechanical mechanism of the inverse magneto-optical Faraday effect, which act on magnetic materials as the effective internal magnetic field (H_F). The magnitude of the effective magnetic field H_F is determined by the magneto-optical susceptibility, which is in the direct dependence on the spin-orbital interaction. The pulsed laser irradiation causes heating and demagnetization that in combination with the laser-induced effective magnetic field can lead to vary of a magnetic state and the remagnetization [3].

The indirect laser impact on magnetic states in nonuniform multilayered magnetic nanostructures can be realized via the laser-induced spin-polarized electron current between magnetic nanolayers [4,5]. In this case the remagnetization of the magnetic junction can be caused by the exchange *s-d* interaction of the laser-injected spin-polarized current with the localized magnetic moment of the injected layer of a magnetic junction. The effective internal magnetic field H_{sd} of that interaction constitutes from two components, $H_{sd} = H_s + H_{inj}$. The first component H_s is related to the *s-d* interaction of the transverse component (with respect to the magnetic moment of the injected layer) of the magnetic moment of the spin-polarized current. The second component H_{inj} is related to the *s-d* interaction of the laser-injected longitudinal spin component (with respect to the magnetic moment of the injected layer) which is characterized by a nonequilibrium distribution. The mentioned effective internal magnetic fields together with laser-induced thermal demagnetization result in the remagnetization, which is accompanied by a tunneling magnetoresistance (TMR) effect.

The dynamics of the laser-induced magnetization is observed with the help of the magneto-optical pump and probe technique. In this technique, the one incident laser pulse stimulates magnetic switching and the second laser beam transmitted or reflected from the magnetic medium serves for image of the laser-induced magnetization. The magnetization image via transmitted or reflected laser beams is based on the magneto-optical Faraday effect or the Kerr effects, respectively [2]. Corresponding magnetization dynamics is described by the Landau-Lifshitz-Bloch equation [6,7] containing temperature dependent parameters of longitudinal and transverse susceptibilities. In the presented paper we have investigated the laser-induced remagnetization and TMR effect in magnetic tunnel junctions consisting of the two TbCoFe-based or the two CoFe-based amorphous ferrimagnetic nanolayers separated by the PrO- based isolating barrier nanolayers. The TbCoFe-based and FeCo-based ferrimagnetic layers are characterized by a perpendicular and single-axis planar magnetic anisotropy, respectively. Based on the magneto-optical measurements by the all-optic pump-probe technique we have studied mechanisms and features of the remagnetization and TMF effects of the tunnel magnetic junctions (TMJ) with intense polarized laser pulses.

2.1. Experiment and Results

The influence of polarized pulsed laser radiation on magnetic states and the conductance of the spin polarized electron current was studied for the magnetic junctions $Al_2O_3/Tb_{22}Co_5Fe_{73}/Pr_6O_{11}/Tb_{19}Co_5Fe_{76}/Al_2O_3$ and $Al_2O_3/Co_{80}Fe_{20}/Pr_6O_{11}/Co_{30}Fe_{70}/Al_2O_3$ with the TbCoFe-based and the CoFe-based ferrimagnetic nanolayers, respectively, separated by the PrO-based isolating barrier layer. The TbCoFe-based and CoFe-based layers are characterized by perpendicular (with respect to a magnetic layer) and single-axis planar magnetic anisotropy, respectively.

The nanolayers $Tb_{22}Co_5Fe_{73}$ and $Co_{80}Fe_{20}$ have a high coercivity and the adjacent nanolayers $Tb_{19}Co_5Fe_{76}$ and $Co_{30}Fe_{70}$ have a low coercivity. The barrier layer represents a large-gap semiconductor similarly to the known [8] case of the MgO-based barrier in the magnetic junction Fe/MgO/Fe. The PrO-based barrier as well as the MgO-based barrier is characterized by a tunneling transparency, a large enough tunneling conductance and the TMR affect under external magnetic field [9]. Corresponding graphic data of the paper [9] are represented in the Figure 1.

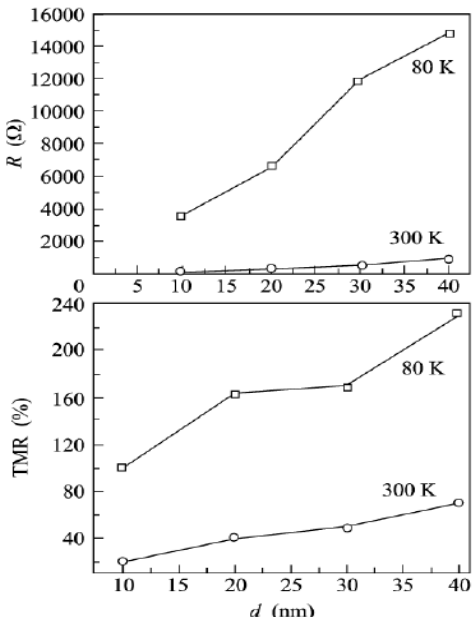

Figure 1. (Upper panel) Tunneling resistance *R* and (lower panel) magnetoresistance TMR of the $SiO_2/Tb_{19}Co_5Fe_{76}/Pr_6O_{11}/Tb_{22}Co_5Fe_{73}/SiO_2$ film structure versus the thickness of the Pr_6O_{11} barrier layer

The magnetic junctions were sprayed by a magnetron deposition technique on plates with sizes 10×14mm and discs with the diameter 110mm made of optical fused quartz with the thickness 1,2mm. Thicknesses of magnetic nanolayers TbCoFe and CoFe constituted 20nm. For the barrier nanolayer Pr_6O_{11} and the cover layer Al_2O_3 thickness constitute 2-3nm and 40nm, respectively. The magnetic junctions with a conductive surface $S = 20\ \mu^2$ are produced by a photolithography technique on the plates with sizes 10-14mm. The edge of plates through which the current was imputed to the tunnel contacts TbCoFe and CoFe was covered by platinum. The contact zone and conductive magnetic strips also were protected by the Al_2O_3 cover with thickness near 40nm.

The mechanisms of the impact of pulsed laser radiation on magnetic states and remagnetizating of the magnetic junctions were studied with the help of linearly and circularly polarized picosecond pulses (pump pulses) with pulse duration about τ_i = 80 ps for a Nd-YAG laser (with a central wavelength λ_0 =1.06μ) and the probe single linearly polarized pulses of the He-Ne laser (with λ_0=1630nm), that was used for imaging of the magnetization dynamics. The last was determined via the rotation angle of a polarization plane of the magneto-optical Kerr and Faraday effects. Features of the laser-induced magnetic dynamics of the magnetic junctions were researched both with the help of magneto-optical measurements and with the TMR effect.

The magnetic dynamics of the tunneling magnetic junctions was studied by the all-optic pump-probe technique. The corresponding setup is represented in Figure 2.

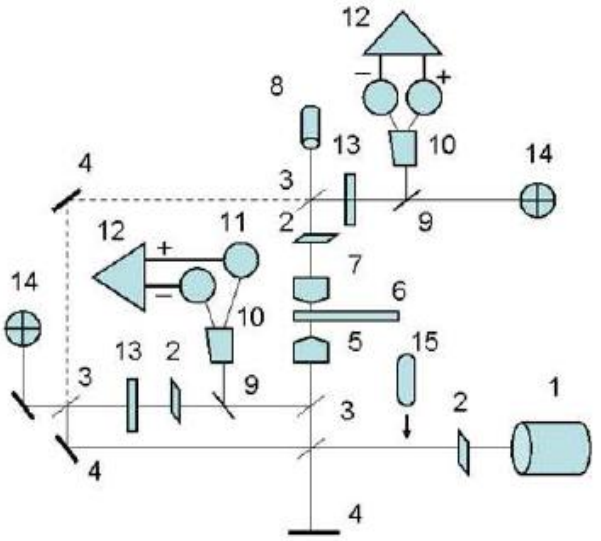

Figure 2. The experimental setup for the optical investigation: the Nd-YAG laser – 1, polarizers − 2, interference mirrors − 3, the total refection mirrors − 4, the standard microscope objective − 5, the substrate with a magnetic film − 6, the special microscope objective − 7, the He-Ne laser − 8, semirefecting mirrors − 9, Senarmon prisms − 10, the sensing photo-diode − 11, differential amplifers − 12, light filters − 13, photodiodes with four active area − 14, the Babinet compensator − 15.

The beam of the Nd-YAG laser 1 with Gaussian energy distribution in its cross-section passed through the polarizer 2 and through the semimirror 3, and then it was directed by 100 % mirror 4 on the special microscope objective 5 with the numerical aperture 0.45. This microscope objective focused laser radiation on the researched film magnetic junction through the substrate 6. Polarized radiation of the He-Ne laser 8 with Gaussian energy distribution in its cross-section was focused by the microscope objective 7 with the numerical aperture 0.5 on the surface of the magnetic junction from its opposite side.

The Nd-YAG laser beam and the beam of the He-Ne laser radiation reflected from the magnetic junction were directed by the interference mirrors 9 on polarization Senarmont prisms 10, where these beams were separated on two beams and registered by the sensitive photodiode 11. The electric signals from the sensitive photodiode were amplified by the differential amplifiers 12. Then these signals were registered by the double-beam oscillo-scope. The laser beam reflected or transmitted through the magnetic junction was directed by the light filters 13 to the polarization Senarmont prism 10. This light filter was used for registration of the He-Ne or the Nd-YAG laser radiation. The polarization twisting of the reflected or the transmitted laser radiation was measured per differential signals from photodiodes 11.

Signals from the photodiode 14 came on the self-focusing microdrivers providing focusing of the microscope objectives 5 and 7 on the magnetic junction surface. By reposition of a substrate with the magnetic junction we could direct the beam of the Nd-YAG laser on the film from the opposite side. The Babinet compensator 15 was used for research of the laser-induced magnetic switching in the magnetic junctions.

For enhancement of the time resolution in picosecond interval the probe polarized beam of the He-Ne laser was formed by the system of 50 % mirrors 3 and 100 % mirrors 4. This beam with the controlled delay (with respect to the pump pulse) was focused on the researched area from the side of the pump laser pulses and opposite side. The polarization twisting of the reflected and transmitted probe laser beam was determined via changing of the signal amplitude, which was registered, by the sensing photodiodes and an oscilloscope.

The one-to-one correspondence between the polarization twisting of the probe radiation of the He-Ne laser and the laser-induced magnetization has allowed to straightforwardly studying the magnetic dynamics of each nanolayers of the investigated magnetic junction $Al_2O_3/Tb_{22}Co_5Fe_{73}/Pr_6O_{11}/Tb_{19}Co_5Fe_{76}/Al_2O_3$. The influence of picosecond laser pulses on magnetic nanolayers $Tb_{22}Co_5$ Fe_{73} and $Tb_{19}Co_5Fe_{76}$ is determined by physical characteristics of laser radiation including its intensity, polarization, pulse duration, and by the magnetic structure of the magnetic layers of the magnetic junctions.

The measurement data concerning the time dynamics of the laser-induced magnetization in the magnetic junctions (with the help of the optical setup Figure 2) are represented in Figure 3.

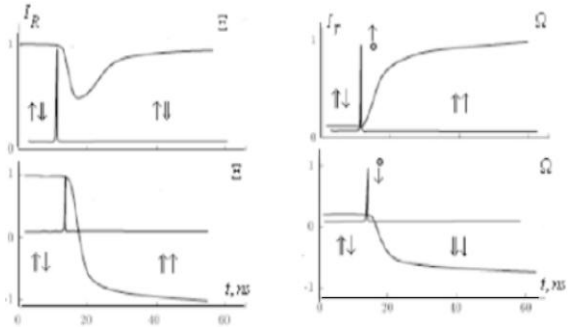

Figure 3. The dynamics of the signals *IR* and *IT* of the He-Ne laser beams, reflected from the low-coercive magnetic nanolayer Tb19Co5Fe76 and transmitted trough magnetic nanolayers, respectively, for the magnetic junction $Al_2O_3/Tb_{22}Co_5Fe_{73}/Pr_6O_{11}/Tb_{19}Co_5Fe_{76}/Al_2O_3$ with different initial magnetization configuration under linearly (Ξ) and circularly (Ω) polarized picoseconds (time duration τ_i = 80 ps) pulsed radiation (dot curves) of the Nd-YAG laser with the intensity I_i = 300 MW/cm^2 at temperature T = 300 K. Single and double arrows denote magnetization directions of the low and high-coercive nanolayers $Tb_{19}Co_5Fe_{76}$ and $Tb_{22}Co_5Fe_{73}$, respectively. The irradiated magnetic nanolayer is determined by the first arrow along the time axis. The single arrow with a circle denotes the direction of the effective magnetic field H_F, which is induced by circularly polarized laser pulses.

In Figure 3 the time evolution curves of photodiode signals for the reflected (the intensity I_R) and transmitted (the intensity I_T) probe laser pulses one-to-one image the remagnetization of the magnetic nanolayers under picoseconds linearly and circularly polarized pump pulses of the Nd-YAG laser.

As it visible from curves on the left in Figure 3 (which corresponds to the linear polarization picosecond pump pulses), the laser-induced remagnetization occurs in the magnetic nanolayer adjoint to an irradiated magnetic nanolayer at the initial antiparallel magnetizations of magnetic nanolayers. Such the magnetic reversal is caused by the effective internal magnetic field H_{sd} of the exchange interaction between the laser-induced spin-polarized electron current through the tunnel barrier and the lattice magnetization together with a laser-induced thermal demagnetization.

The strong enough intensity of the pump laser radiation and small enough its pulse duration constitute necessary conditions for the above-mentioned remagnetization. If the magnetic junction is irradiated by the linearly polarized laser pulses on the side of low-coercive nanolayer the density of the spin-polarized current can be less than its threshold density and therefore the remagnetization not occurs as it represented on the top curve on the left in Figure 3. At the irradiation on the side of the high-coercive nanolayer the density of the spin-polarized current is increased and it can exceed the threshold values of the remagnetization (the curve on the bottom is located in the left of Figure 3).

Curves on the right side in Figure 3 correspond to the circularly polarized pumping picosecond laser pulses. In this case, the laser-induced remagnetization of magnetic layers can be caused both the effective internal magnetic field H_{sd} and the effective internal magnetic field H_F of the magneto-optical inverse Faraday effect together with the laser-induced thermal demagnetization. Usually, the threshold intensities of the pump laser radiation stimulating the remagnetization via the laser-induced effective magnetic fields H_{sd} and H_F are different. Therefore, if such threshold intensity is less for the field H_{sd}, then the remagnetization via the laser-induced spin-polarized electron current passing from the high- to low-coercive magnetic nanolayer can amplifies the remagnetization by the magnetic field H_F, as it is represented in the top curve on the right. If the above-mentioned circularly polarized laser pulses induces the internal magnetic field H_F directed toward the magnetization of high-coercive nanolayer, then the magnetic field H_{sd} vanishes and the remagnetization is completely determined by the magneto-optical inverse Faraday effect (bottom curve on the right Figure 3).

The laser-induced TMR effect was studied on the TbFeCo-based magnetic junction $Al_2O_3/Tb_{22}Co_5Fe_{73}/Pr_6O_{11}/Tb_{19}Co_5Fe_{76}/Al_2O_3$ and the CoFe-based magnetic junction $Al_2O_3/Co_{80}Fe_{20}/Pr_6O_{11}/Co_{30}Fe_{70}/Al_2O_3$. These junctions, as it was above denoted, are characterized by a large tunneling conductance and a TMR effect (which is determined by the relative resistance change under remagnetization). In our opinion, similarly to the case of the MgO-based magnetic junctions, it is connected with a match between propagating electron–electron states in magnetic layers and evanescent states in the barrier layer near the Fermi level (see [8]). That provides couple of an electron state from the TbCoFe into the PrO and out of the PrO into the TbCoFe. It is exhibited in the large TMR effect under external magnetic field, which for the TbCoFe-based magnetic junction reach 70% at 300 K and 240% at 80 K [9]. Corresponding field dependences are represented in the Figure 4.

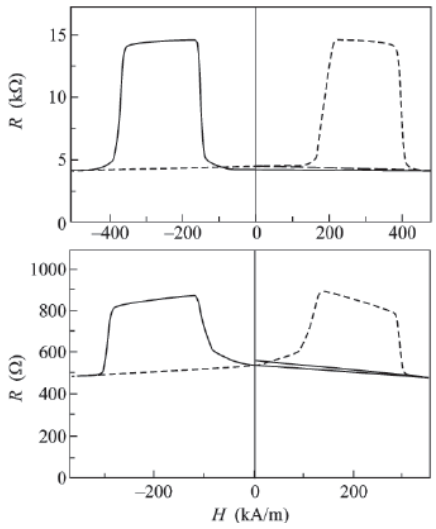

Figure 4. Resistance of the $SiO_2/Tb_{19}Co_5Fe_{76}/Pr_6O_{11}/Tb_{22}Co_5Fe_{73}/SiO_2$ tunneling contact versus the applied magnetic field at T = 80 K (upper panel) and T=300 K (lower panel)

The laser-induced remagnetization and TMR effect can be caused by the effective internal magnetic fields H_F of the inverse Faraday effect and H_{sd} of the exchange $s-d$ interaction between the lattice spins and the spin current stimulated by the power enough polarized pulsed laser radiation [5,18,21] together with the laser-induced demagnetization. The last precedes the mentioned magnetic switching. The laser-induced thermal magnetization should be sufficient for the remagnetization by the effective magnetic field. It assumes the suitable combinations of the laser pulse duration and intensity.

The TbCoFe-based and CoFe-based TMJ are characterized by the large enough magneto-optical susceptibility, a spin-orbital interaction, an electron spin polarization and thermal susceptibility of their magnetic nanolayers, that provide their laser-induced remagnetization. For the TbCoFe-based magnetic junction possessing by a perpendicular magnetic anisotropy the essential role in the laser-induced magnetization belongs to the effective internal magnetic field H_F of the magneto-optical inverse Faraday effect, which is collinear to the magnetic anisotropy axis. The last can be amplified by the laser-induced effective magnetic field H_{sd}. The corresponding remagnetization results in resistance switching (the laser-induced magneto-resistance effect without an external magnetic field). In the case of the CoFe-based magnetic junction, possessing by a planar magnetic anisotropy axis, the impact of the laser-induced magnetic field H_F, perpendicular to this axis, vanish and the dominant role in the laser-induced magnetization can belong to the effective magnetic field H_{sd} related to the laser-induced spin-polarized electron current.

The above mentioned laser-induced remagnetization and TMR effect experimentally was studied on the TbCoFe-based and CoFe-based TMJ with different initial magnetic configurations under linearly and circularly

polarized picosecond laser pulses. Corresponding results are represented in Figure 5.

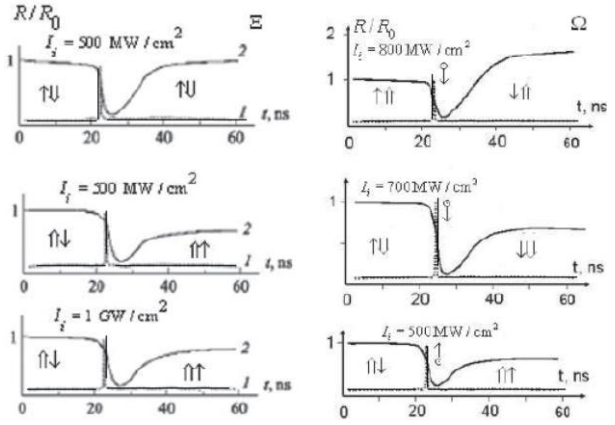

Figure 5. The dynamics of the R/R0 of the TMJ $Al_2O_3/Tb_{22}Co_5Fe_{73}$ /$Pr_6O_{11}/Tb_{19}Co_5$ Fe_{76}/Al_2O_3 (all curves except of the bottom curve on the left) and $Al_2O_3/Co_{80}Fe_{20}/Pr_6O_{11}/C_{30}Fe_{70}/Al_2O_3$ (the bottom curve on the left) with different magnetization configurations of magnetic nanolayers excited by linearly (denoted as Ξ on the left) and circularly (denoted as Ω on the right) polarized laser pulses (dot curves) with the duration τ_i= 80 ps at different temperatures T and intensity I_i. Curves on the left and the top curve on the right correspond to the temperature T = 80 K and two bottom curves on the right correspond to temperature T = 300 K. Single and double arrows denote magnetization directions of the low- and high-coercive nanolayers $Tb_{19}Co_5$ Fe_{76}/Al_2O_3, $Co_{80}Fe_{20}$ and C $_{30}Fe_{70}$, Co30Fe70, respectively. The irradiated nanolayers is determined by the first arrow along the temporary axis before the laser pulse. The single arrow with a circle denotes the direction of the effective magnetic field H_F, which is induced by the circularly polarized laser pulses.

The remagnetization and resistance switching of the magnetic junctions with the line-polarized picoseconds laser pulses occur under the effect of the laser-induced thermal demagnetization and effective magnetic field H_{sd} in the magnetic nanolayer adjacent to an irradiated nanolayer. The laser radiation intensity and the induced field H_{sd} should be sufficient for the remagnetization. The field H_{sd} is directly dependent on the laser-induced spin-polarized current; therefore, its value is significantly larger at the laser irradiation of the high-coercive nanolayer than low-coercive nanolayer and can be insufficient for the magnetic switching.

In the case of the linearly polarized pulsed laser irradiation, the remagnetization and laser-induced TMR effect of the magnetic junctions occur only under the action of the laser-induced effective magnetic field H_{sd} and the laser-induced thermal demagnetization. Corresponding time dynamics of the resistance switching for the antiparallel initial magnetization configuration is represented by the curves on the left in Figure 5. As it is visible from the top curve on the left, the laser irradiation of the low-coercive nanolayer $Tb_{19}Co_5Fe_{76}$ does not causes the remagnetization of the adjacent nanolayer and resistance switching, since the laser-induced spin-polarized electron current and the corresponding field H_{sd} are insufficient for the magnetic switching. However, the laser irradiation of the high-coercive nanolayers $Tb_{22}Co_5Fe_{73}$ and $Co_{80}Fe_{20}$ causes such remagnetization and resistance switching, since laser-induced spin-polarized electron current and the corresponding field H_{sd} became sufficient for the magnetic switching, that is visible from two bottom curves on the left in Figure 5.

For the circularly polarized picosecond pulsed laser irradiation the remagnetization and laser-induced TMR effect of the magnetic junctions occur under the total action of the laser-induced effective magnetic fields H_F and H_{sd} together with the laser-induced thermal demagnetization. Corresponding time dynamics of the resistance switching for the different initial magnetization configurations is represented by the curves on the right in Figure 5. As it is visible from the top curve on the right, at parallel initial magnetization configuration, the circularly polarized pulsed laser irradiation with the helicity, corresponding to the field H_F antiparallel to the initial magnetization of the irradiated low-coercive nanolayer Tb19Co5Fe76, can cause its remagnetization and resistance switching. In this case, the field H_{sd} is absent. In the case of antiparallel initial magnetization configuration, as it is visible from the middle curve on the right in Figure 5, the circularly polarized pulsed laser irradiation with the helicity, corresponding to the field H_F antiparallel to the initial magnetization of the irradiated low-coercive nanolayer Tb19Co5Fe76 can cause its remagnetization and resistance switching. The laser-induced spin-polarized current and efficient magnetic field H_{sd} are small with respective to the dominant field H_F.

For the antiparallel initial magnetization configuration, the circularly polarized pulsed laser irradiation with the helicity, corresponding to the field HF parallel to the initial magnetization of the irradiated high-coercive nanolayer $Tb_{19}Co_5Fe_{76}$ can cause the remagnetization of the adjacent magnetic caused by both a sum of the magnetic fields H_F and H_{sd}. It results in the resistance switching, as it is visible from the bottom curve on the right in Figure 3. In this case it is turned out, that the laser-induce magnetic field H_{sd} gave an essential contribution in the remagnetization.

2.2. Analysis of Results

The laser-induced magnetization dynamics of the explored tunnel magnetic junction, including the temperature dependence of the magnetization magnitude, can be described by the macroscopic Landau-Lifshitz-Bloch (LLB) equation [6]

$$\frac{\partial \mathbf{m}_i}{\partial t} = -\tilde{\gamma}\left[\mathbf{m}_i \times \mathbf{H}^i_{eff}\right] + \frac{\tilde{\gamma}\alpha_{||}}{m_i^2}\left[\mathbf{m}_i \cdot \left(\mathbf{H}^i_{eff} + \boldsymbol{\varsigma}^i_{||}\right)\right]\mathbf{m}_i - \frac{\tilde{\gamma}\alpha_{\perp}}{m_i^2}\left[\mathbf{m}_i \times \left[\mathbf{m}_i \times \left(\mathbf{H}^i_{eff} + \boldsymbol{\varsigma}^i_{\perp}\right)\right]\right] \quad (1)$$

which was derived [7] in a mean-field approximation from the classical Fokker–Planck equation for individual spins interacting with a heat bath. In (1) $\tilde{\gamma} = \gamma/(1+\lambda^2)$, where γ is the gyromagnetic ratio and λ is a microscopic parameter that characterizes the coupling of the individual atomistic spins with the heat bath. It is visible from (1), that a spin polarization m_i has no constant length and is temperature dependent. The coefficients $\alpha_{||}$ and $\alpha_{\perp}$ are dimensionless longitudinal and transverse damping parameters. Thermal fluctuations are included as an additional noise terms $\varsigma^i_l(t)$ with $l = (\perp, ||)$ and

$$\left\langle \varsigma_l^{i,\eta}\varsigma_l^{i,\mu}\right\rangle = \frac{2k_BT}{\tilde{\gamma}M_s^0\Delta^3}\delta_{\nu\eta}\delta_{ij}\delta(t) \qquad (2)$$

where i, j denote lattice sites and η, μ denote the Cartesian components. Here, Δ^3 is the volume of the micromagnetic cell and M_s^0 is the value of the spontaneous magnetization at zero temperature. The damping parameters below and above the magnetic phase transition temperature T_M are described by the expressions $\alpha_{||} = 2T/(3T_M)$, $\alpha_{\perp} = \lambda\left(1 - T/T_M\right)$ and $\alpha_{\perp} = \alpha_{||} = 2\lambda T/(3T_M)$, respectively.

The effective magnetic field can be written as $H_{eff}^i = H_{l-ind} + H_{a-ex}^i$. Here the first ingredient H_{l-ind} is caused by the laser-induced electron excitations which includes both the effective internal magnetic field of the inverse magneto-optical Faraday effect (H_F) and the internal magnetic field (H_{sd}), generated by the s−d exchange interaction of laser-injected spin-polarized currents with localized spins of magnetic lattice in the spatially inhomogeneous magnetic junction. The second ingredient $H_{a-ex}^i = H + H_a^i + H_{ex}^i$ is given by

$$H_{a-ex}^i = \begin{cases} \frac{1}{2\tilde{\xi}_{||}}\left(1-\frac{m_i^2}{m_{eq}^2}\right)m_i, & T<T_M; \\ -\frac{1}{2\tilde{\xi}_{||}}\left(1+\frac{3T_m m_i^2}{5(T-T_M)}\right)m_i, & T\geq T_M, \end{cases} \qquad (3)$$

where the susceptibility $\tilde{\xi}^l = \partial m_l/\partial H_l$. The anisotropy and exchange fields are given by

$$H_a^i = -\frac{\left(m_x^i e_x + m_y^i e_y\right)}{\tilde{\xi}_{\perp}}$$

and

$$H_{ex}^i = -\frac{A}{m_e^2}\frac{2}{M_s^0\Delta^2}\sum_{j\in \text{neigh (i)}}\left(m_j - m_i\right)$$

respectively.

Within the context of the LLB equation, field components parallel to the local magnetic moment can change the length of the magnetization vector. In the limit, $T \to 0$ the longitudinal damping parameter $\alpha_{||}$ vanishes and with $|m| = m_{eq}(0)$ the LLB equation goes over to the usual Landau–Lifshitz–Gilbert (LLG) equation [22]. The temperature dependent parameters in (1), i.e. longitudinal, transverse susceptibilities, and the temperature variation of the magnetization, $\chi_{||}(T)$, $\chi_{\perp}(T)$ and $m_e(T)$ are determined using an Langevin dynamics combined with the LLG equation for each spin, i.e., by its stochastic modification [6].

$$\boldsymbol{S}_i = -\frac{\gamma}{(1+\lambda^2)\mu_S}\left[\boldsymbol{S}_i\times\boldsymbol{H}_i + \lambda\boldsymbol{S}_i\times\boldsymbol{S}_i + (\boldsymbol{S}_i\times\boldsymbol{H}_i)\right] \qquad (4)$$

where the internal field $\boldsymbol{H}_i = \partial\boldsymbol{H}/\partial\boldsymbol{S}_i + \boldsymbol{\xi}_i(T)$. Thermal fluctuation of the mentioned parameters are include as an additional noise term in the internal field with $<\chi_i(t)> = 0$ and $<\chi_i^k(t)\chi_j^l(t)> = 2\delta_{ij}\delta_{kl}\lambda k_B T\mu_s/\gamma$.

The system (1) and (4) has solution for the magnetization $m(t)$, which at the temperatures close to the magnetic phase transition temperature T_M tends to zero (that means a demagnetization process). Then at cooling, one tends to the magnitude with the sign opposite to initial value (that means the magnetic switching). The system (1) and (4) determined the conditions for parameters providing the magnetic switching. It turns out that the magnetic switching only occurs within a narrow range of parameters for the laser pulse. The realization of the magnetic switching assumes the suitable combinations of laser pulse duration and intensity.

The component H_{sd} of the effective magnetic field H_{eff} in (1) expresses via the s−d-exchange interaction U between the spin-polarized current and the lattice magnetization m as

$$H_{sd}(x,t) = -\frac{\delta U_{sd}}{\delta m(x,t)} = -\alpha\frac{\delta}{\delta m(x,t)} \times \int_0^L dx' m_{el}(x',t)m(x',t),$$

where $m_{el}(x,t)$ is the magnetization of the laser-induced spin-polarized current and L is thick of a magnetic nanolayer of the tunnel magnetic junction. Since the magnetization $\boldsymbol{m} = \boldsymbol{m}(\boldsymbol{x},t)$ is connected with the magnetization flux density $\boldsymbol{J}$ by the continuity equation

$$\frac{\partial \mathbf{m}_{el}}{\partial t} + \frac{\partial \boldsymbol{J}}{\partial \boldsymbol{x}} + \gamma\alpha\left[\boldsymbol{m}_{el}\times\boldsymbol{m}\right] + \frac{\boldsymbol{m}_{el} - \bar{\boldsymbol{m}}_{el}}{\tau} = 0 \qquad (5)$$

(where $\bar{\boldsymbol{m}}_{el}$ is an averaged magnetization, τ is a relaxation time with respect to a local equilibrium state), then the effective magnetic field $H_{sd} = H_{sd}(\boldsymbol{J})$, i.e., it depends on the magnitude of the laser-induced current and the intensity of laser pulses.

The continuity condition of the magnetization flux near to the interface between continuity adjacent magnetic layers determines the boundary conditions for (1) that allows describing the magnetization dynamics under the laser-induced spin-polarized electron current. The continuity condition for the traverse components of the magnetization flux near to interface between adjacent magnetic layers result in a transfer of torque moment from labile electrons to lattice moments. The corresponding

transverse component ($H_{sd,\perp}$) of internal magnetic field H_{sd} can result in magnetic switching in a small region near to the interface at excess of threshold intensity of laser pulses [5]. This spin torque effect assumes spin dissipation.

At the same time, the continuity condition for the longitudinal components of the magnetization flux through the interface in (1) result in the longitudinal component $H_{sd,\|}$ of the magnetic field H_{sd} caused by the nonequilibrium spin polarization of spin-polarized electrons of laser-injected through the interface into an adjacent magnetic layer. The magnetic field $H_{sd,\perp}$ (independent on the spin dissipation) results in the magnetization switching in bulk of the magnetic layer at a threshold magnitude of the laser intensity.

Thus, due to (1) the change of the effective magnetic field H_{eff} can result in the magnetization reorientation and switching. For the single magnetic nanolayer the effective magnetic field is caused only by the effective field H_{i-ind} related to the optic-magnetic excitations. For the tunneling magnetic junction the laser-induced effective magnetic field H_{i-ind} also includes magnetic field H_{sd} related to the laser-induced spin-polarized flux, playing the essential role in magnetization and switching processes. The last field is the sum $H_{sd} = H_{sd,\perp} + H_{sd,\|}$, where the first and second terms are related to the transverse and longitudinal components of the spin flux, respectively.

The effective field $H_{sd,\perp}$ related to the exchange *s-d* interaction between the lattice magnetization and the transverse component of the laser-induced spin magnetic flux damping near the magnetic interface. The effective field corresponds to the scattering of spin-polarized electrons on localized magnetic ions accompanying by the action of the torque T on the magnetic lattice. Spin magnetic momentums of the spin-polarized current and the lattice are aligned on the distance l , i.e., the transverse component of the total magnetic flux is completely damped. This torque (corresponding to the continuity condition of the total magnetic flux) is determined via the spin electron polarization vector p_{cur} and magnetization vector m by the vector product [4,5].

$$T = \sigma I[m \times m \times p_{cur}]/|m|$$

where σ is the constant depended on the efficiency of the scattering processes in the thin nanolayer, I is pro-proportional to the density of the laser-induced current of spin-polarized electrons. The increase of the laser-induced current density of spin-polarized electrons to some critical value (on the order 10^7 A/cm^2) causes the large enough torque for the magnetic switching near the junction interface.

The effective field $H_{sd\|}$ is related to the longitudinal component of the total magnetic flux, consisting of laser-induced spin-polarized current and lattice magnetic components, which passes in the low-coercive layer on the spin diffusive depth (on the order 10 nm). This field is generated by the exchange *s-d* interaction of the non-equilibrium spin polarization state with the lattice magnetization (that is caused by the nonequilibrium distribution of the laser-induced electrons between spin subbands in the low-coercive magnetic layer) with the lattice magnetization. The field $H_{sd\|}$ is characterized by the direct dependence on the density of the laser-induced spin-polarized electron current. It is always parallel in the magnetization of the strongly coercive magnetic layer. Therefore, the increasing of the current density to some critical value is accompanied by the increasing of $H_{sd\|}$ and magnetic switching if the magnetization directions of adjacent magnetic nanolayers are antiparallel.

3. Impact of Laser-Induced Heating on Remagnetization Dynamics

Features of the laser-induced thermal effect on a magnetization dynamics and remagnetization of ferrimagnetic layers can be related to different temperature magnetization dependences and substantially different speeds of thermal demagnetizations of ferrimagnetic sublattices. The distinction of temperature behaviors of ferrimagnetic lattices manifests in existence of magnetic and angular momentum compensation points, where temperature dependences of a sublattice magnetization and a sublattice angular momentum intersect. The ferrimagnetic remagnetization is determined by features of the temperature behavior of sublattice magnetization near the compensation points. Depending on their composition, ferrimagnetic can exhibit a magnetization compensation temperature T_M where the magnetizations of ferrimagnetic sublattices cancel each other, and similarly, an angular momentum compensation temperature T_A where the net angular momentum of the sublattices vanishes.

Substantially different timescales of the laser-induced thermal demagnetization of the ferrimagnetic sublattices result in emerging the effective bias magnetic field acting on the demagnetized sublattice on the side of again not demagnetized sublattice. It leads to the transient ferromagnetic state with parallel magnetizations of sublattice that together with the exchange interaction relaxation can cause a magnetization reversal of the sublattices.

The mentioned laser-induced thermal impact on the magnetization dynamics and the remagnetization of ferrimagnetic nanolayers are observed in rare earth-3d transition metal (RE-TM) ferrimagnetic compounds. Such compounds, specifically, GdFeCo, are widely used materials for magneto-optical recording, and represent the suitable physical models for study the above-mentioned temperature dependent magnetization in ferrimagnetic nanolayers.

3.1. Magnetization Dynamics across Compensation Points

The dynamics of the laser-induced remagnetization of ferrimagnetic nanolayers substantially depends on the

temperature magnetization behavior their sublattices [13,14]. The remagnetization speed at transition across the across the magnetization compensation temperature T_M is in direct relation on a frequency and a magnetic precession damping. Considerable increase of these quantities in the framework of the modified Landau-Lifshitz model occurs at passage of the angular compensation temperature T_A.

The main regularities of the magnetization dynamics for ferrimagnetic nanolayers exhibit in the ferrimagnetic physical model based on rare eath-3d (RE) transition metal (TM) ferrimagnetic composed of RE and TM sublattices with antiparallel magnetizations which can be represented by the ferrimagnetic compound GdFeCo. The dynamics of the magnetization m_i (i =RE,TM) of this ferrimagnetic is described by the equation

$$\frac{\partial \boldsymbol{m}_i}{\partial t} = -|\gamma_i|\left[\boldsymbol{m}_i \times \boldsymbol{H}_i^{eff}\right] + \frac{\alpha_i}{|m_i|}\left[\boldsymbol{m}_i \times \frac{\partial \boldsymbol{m}_i}{\partial t}\right], \quad (6)$$

$$\boldsymbol{H}_{i(j)}^{ex} = -\chi_{ex}\boldsymbol{m}_{(j)i}, \quad i, j = (\mathrm{RE,TM})$$

with gyromagnetic ratio and the Gilbert damping parameter given by $|\gamma_i| = g_i\mu_B/\hbar$ and $\alpha_i = |\lambda_i|/|\gamma_i|m_i$, respectively. Here λ_i is the Landau-Lifshitz damping parameter [13]. The quantity χ_{ex} is a reversible magnetic susceptibility, coupling the magnetization of the sublattice RE (TM) with external magnetic field acting on the sublattice (TM) RE.

Solutions of the system (6) are characterized by frequencies of ferromagnetic (ω_{FMR}) and exchange (ω_{ex}) resonances [23]

$$\omega_{FMR} = \gamma_{eff}H^{eff}, \quad \omega_{ex} = \chi_{ex}|\gamma_{RE}||\gamma_{TM}|A(T) \quad (6a)$$

where an effective gyromagnetic ratio γ_{eff} is the function of temperature T and is determined via the sublattice magnetization as

$$\gamma_{eff}(T) = \frac{m_{RE}(T) - m_{TM}(T)}{\frac{m_{RE}(T)}{|\gamma_{RE}|} - \frac{m_{TM}(T)}{|\gamma_{TM}|}} = \frac{A_0}{A(T)} \quad (7)$$

Here $m(T)$ and $A(T)$ are temperature dependent the net magnetization and angular moment, A_0 is constant under the assumption of Landau-Lifshitz damping parameter being independent of temperature. At tending temperature T to the angular momentum compensation temperature T_A ($A(T) \to 0$) the effective giromagnetic ratio (7) sharply increase. Similar increasing is observed for the damping parameter of a magnetic precession.

$$\alpha_{eff}(T) = \frac{\frac{\lambda_{RE}(T)}{|\gamma_{RE}|^2} + \frac{\lambda_{TM}(T)}{|\gamma_{TM}|^2}}{\frac{m_{RE}(T)}{|\gamma_{RE}|} - \frac{m_{TM}(T)}{|\gamma_{TM}|}} = \frac{A_0}{A(T)} \quad (8)$$

Equations (7) and (8) indicate a divergence of both the precession frequency and Gilbert damping parameter of the FMR mode at the temperature T_A. Moreover, from the equation (7), one can be notice that at the temperature T_A, the FMR frequency becomes zero. In contrast, the equation (6a) indicates that the exchange resonance branch soften at the angular momentum compensation temperature T_A, where the FMR mode diverges.

The mentioned effects of increasing the ferromagnetic frequency and the damping parameter at decreasing the exchange resonant frequency represent the conditions for substantial increase of the remagnetization speed of ferrimagnetic nanolayers under circularly polarized pulsed laser radiation. The damping of the exchange interaction resonant frequency accompanies by the interaction damping. That results in the acceleration of the magnetization reverse of these sublattices under the internal effective magnetic field of the inverse magneto-optical Faraday effect at passage the magnetization compensation temperature.

Character features of the impact of laser-induced pulsed heating on the dynamics and the remagnetization of a ferrimagnetic nanolayer also can observed under the linear polarized laser radiation in an external magnetic field at temperatures above the magnetization compensation point T_M. In this case the ferrimagnetic magnetization m is directed along the effective magnetic field $H^{eff} = H_{ex} + H_a + H_s$, where H_a and H_s are a magnetocrystallin and a form anisotropy, respectively. The laser thermal pulses result in the change of the field H^{eff} that causes the magnetization precession round a changed equilibrium axis. The appropriate temperature behavior of the ferrimagnetic nanolayer based on compound $Gd_{22}Fe_{74.6}Co_{3.4}$ is represented in Figure 5.1 [13].

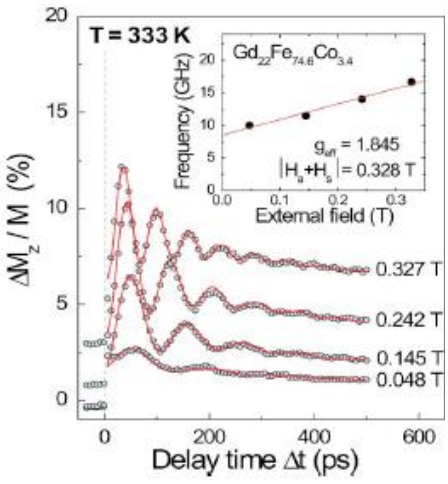

Figure 5.1. Magnetization precession in GdFeCo as a function of the applied external field. Inset shows the field dependence of the precession frequency. Note that the sample temperature presented here includes the temperature increase induced by the pump heating

The solutions of the equalization (6) for the magnetization dynamics are characterized by damping (as the result of an electron-phonon interaction) by magnetization vibrations which amplitudes are in a direct relation with the external magnetic field H_{ex}. It turns out,

that the ferrimagnetic sublattice TM gives a basic contribution to this magnetization. The expression for the square of frequency ω of the magnetization precession [23]

$$\omega^2 = \left(\frac{\gamma_{eff}}{(1+\alpha_{eff}^2)} \right)^2 \left((H_{ex}\cos\theta_{ex} + |H_S + H_a|)^2 - (H_{ex}\sin\theta_{ex})^2 \right) \quad (9)$$

(θ_{ex} is a angle between the external magnetic field and an easy magnetic anisotropy axis) allows to determine the internal magnetic field $H_S + H_a$ and also the effective gyromagnetic relation and damping parameter in the ferrimagnetic nanolayers.

At initial temperatures below the magnetization compensation temperature T_M a thermal relaxation after the pulsed laser heating, can be accompanied by a transition of ferrimagnetic through the temperature T_M with reversing of magnetization of each sublattices RE and TM under the external magnetic field. Such magnetization reversal companies by the phase change of magnetization vibrations (Figure 6) [13].

In the ferrimagnetic nanolayer GdFeCo at temperatures $T < T_M$, the magnetization m_{RE} of the sublattice RE (Gd) is larger than the magnetization m_{TE} of the sublattice TM (FeCo) and it is directed along the external magnetic field H_{ex}. At $T > T_M$ the magnetization $m_{TM} > m_{RE}$ and varies its direction along the external magnetic field H_{ex}, as it is visible in the inset of Figure 6.

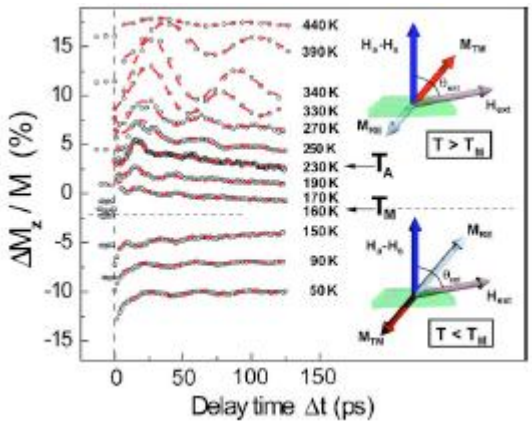

Figure 6. Temperature dependence of coherent precession of the magnetizations in GdFeCo, measured at an external field H_{ex} = 0.29 T. Around 160 K magnetic compensation T_M of the ferrimagnetic system occurs. The inset shows the alignment of the RE-TM system under an external applied field, below and above T_M

The magnetization reverse under the pulsed laser-induced heating and the external magnetic field are in direct relation on the frequency and the damping of the magnetization precession. It appears [13,14], that features of the temperature dependence of the magnetization procession frequencies near the angular momentum compensation temperature T_A determine their temperature behavior near magnetization compensation temperature T_M. In the temperature interval [T_A,T_M] the magnetization precession frequency determines by the total action of exchanging interaction between spins of each sublattices RE and TM, as it is visible in Figure 7.

In the temperature interval [T_A,T_M] it is observed the hybridization of the resonant frequencies ω_{FMR} and ω_{ex}, and the magnetization precession frequency at the magnetization compensation temperature T_M attains the significant value, constituting 40 GHz (Figure 7). The effective damping parameter at T_A takes the maximum value remaining large enough in closely approximating point T_M. Changing the composition of the ferrimagnetic (GdFeCo) it is possibly to attain a necessary proximity between compensation points T_A and T_M, providing the rapid remagnetization of the ferrimagnetic nanolayer. For circularly polarized laser pulses, such the remagnetization can occur without an external magnetic field under an effective internal magnetic field of the inverse magneto-optical Faraday effect.

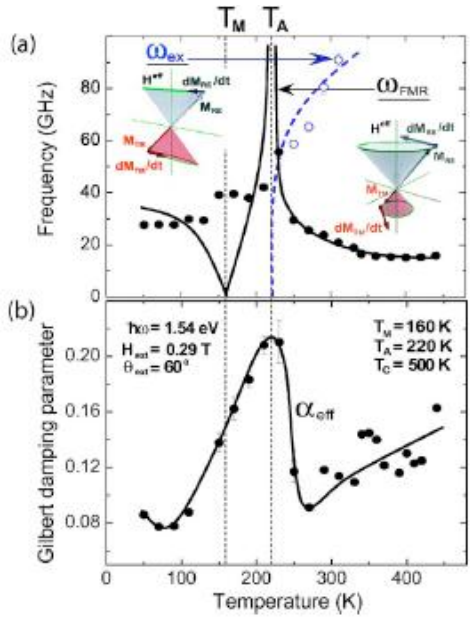

Figure 7. (a) Temperature dependence of the magnetization precession frequencies ω_{FMR} and ω_{ex}. As temperature decreases from 310 K toward T_A, the exchange resonance mode ω_{ex} (open circles) softens and mix with the ordinary FMR resonance ω_{FMR} (closed circles). Since around 230 K both FMR and exchange modes have essentially the same frequency, the frequency indicated at 230 K may represent both the FMR and the exchange resonance modes. The insets show schematically the two modes. (b) Temperature dependence of the Gilbert damping parameter α_{eff}

The thermal action of the laser pulses with heating a ferrimagnetic above the mentioned compensation points results in the effect of the ultra-speed (subpicosecond) remagnetization [14]. This is related to features of the magnetization dynamics of ferrimagnetic sublattices that

is observed with the help of the magneto-optical pump-probe technique. Thermal pumping is provided by pulsed laser irradiation and magnetic responses are imaged with the help of the magnet-optical Faraday effect [16] via the polarization twisting of probing laser pulses. Then the magnetization dynamics depends on the ratio between the applied magnetic field H_{ex} and the temperature dependent coercive field $H_C(T)$ of the ferrimagnetic nanolayer.

Character features of magnetization dynamics of the ferrimagnetic nanolayer under laser thermal pulses of different power are observed for the amorphous ferrimagnetic $Gd_{22}Fe_{74.6}Co_{3.4}$ with the magnetization compensation temperature $T_M = 370$ and the angular momentum temperature $T_A = 420$ K (Figure 8) [14].

The laser-induced pulsed heating the electron subsystem of ferrimagnetic continues by high-speed heating of its spin subsystem with subsequent cooling to an initial temperature, that accompany by thermal changes of magnetizations $m_{RE}(T)$ and $m_{TM}(T)$ of the sublattices RE and TM of the ferrimagnetic GdFeCo. At enough laser radiation intensities the mentioned heating can causes the magnetization reverse of the sublattice under an applied magnetic fields (which can be both an external field and the effective Faraday magnetic field) as it is visible in Figure 8.

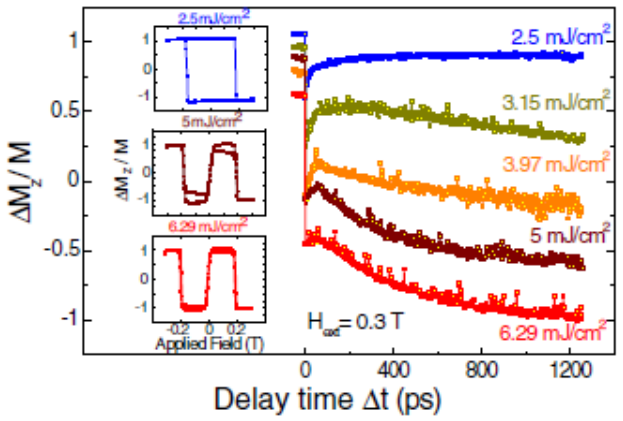

Figure 8. The magnetization dynamics in the ferromagnetic $Gd_{22}Fe_{74.6}Co_{3.4}$ at a room temperature for different energies of the laser pumping [14]. Apt hysteresis loops are represented in the inset

The mentioned magnetization reverse is related to the passage by opposite oriented magnetizations $m_{RE}(T)$ and $m_{TM}(T)$ across the magnetization compensation point T_M in which these magnetizations cancel each other. However, magnetization dynamics at a thermal relaxation can occurs in a variety of ways in the dependence on the relation between the applied field H_{ex} and the temperature dependent coercive field $H_C(T)$ in the temperature interval from the initial room temperature T_{room}, where $H_C(T_{room}) = H_c^{room}$ to the highest temperature T_{high}, where $H_C(T_{high}) = H_c^{high}$, is the condition of the ferrimagnetic remagnetization, as it is visible in Figure 9.

Under the condition $H_{ex} > H_c^{room(high)}$, below the magnetization compensation temperature T_M the magnetization m_{RE} of the Gd sublattice is parallel to the magnetization m_{TM} of the FeCo sublattice and one exceed its on an absolute value. Under the impact of the laser-induced thermal pulse a temperature increases above the point T_M and the magnetization m_{TM} becomes dominant and parallel to the applied magnetic field. After the pump laser, pulse at the temperatures above T_M the magnetization m_{TM} relaxes in the line its initial state. Subsequent cooling below the temperature T_M results in recovery the initial magnetization state of the ferrimagnetic nanolayer.

The magnetization dynamics is substantially different at $H_{ex} < H_c^{room}$ and $H_{ex} > H_c^{high}$, when the initial coercive field exceeds the applied magnetic field. In this case, the laser thermal pulse causes the remagnetization above the magnetization compensation point T_M without return to the initial magnetization state at cooling system to the room temperature T_{room} (Figure 9 (b) B). This implies that at $H_{ex} < H_c^{room}$ after the remagnetization a thermal relaxation not changes the magnetization direction of the ferrimagnetic nanolayer.

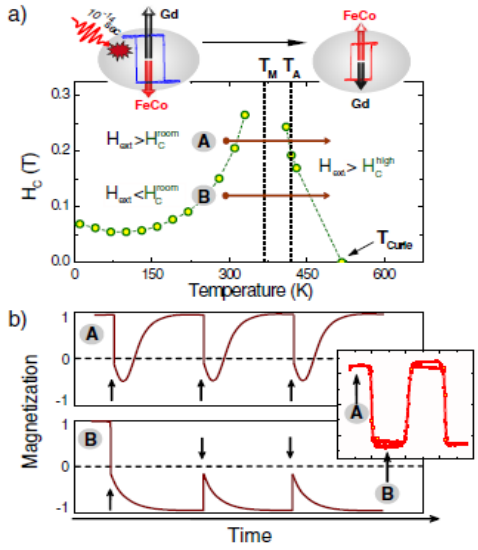

Figure 9. (a) Temperature dependence of the effective coercive field H_C in the $Gd_{22}Fe_{74.6}Co_{3.4}$ nanolayer. The inset of the figure shows schematically the ferrimagnetic system in an applied magnetic field below and above T_M Depending on the strengths of the applied magnetic field, two different dynamic regimes can be distinguished: (A) for $H_{ex} > H_{room}$ and (B) for $H_{ex} < H_{room}$. (b) Qualitative description of the magnetization dynamics, induced by pump laser pulses

The high remagnetization speed of the ferrimagnetic nanolayer under the laser-induced thermal pulses determined by the large effective gyromagnetic ratio

γ_{eff} with a singularity at the angular momentum compensation temperature T_A of the sublattices RE and TM. The magnetization dynamics for the ferrimagnetic $Gd_{22}Fe_{74.6}Co_{3.4}$ is characterized by the subpicosecond remagnetization, as it is visible in Figure 10, where results of the magneto-optical Faraday-based measurements are represented.

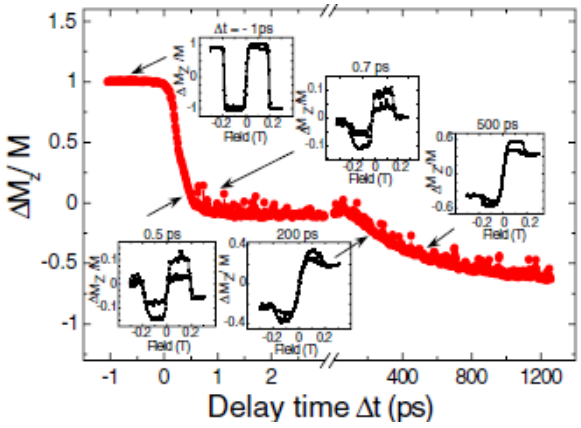

Figure 10. Transient magnetization reversal dynamics measured for a pump fluence of 6:29 mJ/cm^2. Insets show hysteresis loops measured at distinct pump-probe delays. The loops demonstrate the magnetization reversal after about 700 fs

The laser ultra-speed excitation of the magnetic moments of the atoms Fe in the sublattice FeCo occures via conduction electrons. For the sublattice Gd, the 4f electrons give a main contribution in a magnetic atomic moment, whereas the contribution of 5d6s conduction electrons constitute only 9 %. In this case the ultra-speed laser excitation of the magnetic atomic moment occurs via 5d electrons, which characterized by the strong exchange interaction with the localized 5d electrons. The energy of this exchange couple corresponds to subpicosecond times, on which the mentioned remagnetization of the Gd sublattice.

3.2. The Fast Remagnetization Across Transient Ferromagnetic-Like State

The pulsed thermal impact of the layer radiation on the magnetization of the ferrimagnetic nanolayer occurs via the laser interaction with each of its sublattices. Therefore, in whole, the magnetization dynamics is determined by the magnetization dynamics of each of the ferrimagnetic sublattices. At the laser-induced excitation of the spin subsystem in time-scales that correspond to an antiferromagnetic exchange interaction between sublattices (i.e., in the interval, 10-100 fs) the system is some time in a strong nonequilibrium magnetic with the disturbed equilibrium dynamic correlation between the sublattices. That implies the possibility of a disturbance of the equilibrium magnetization configuration at the magnetization relaxation of the ferrimagnetic system to a equilibrium state.

The lather-induced thermal demagnetization of each of the ferrimagnetic sublattices occurs over different periods. Whereas in the ferrimagnetic under the applied magnetic field H_{ex} the change of the magnetization direction occurs after the sublattice demagnetization then in the period between such demagnetization moments the ferrimagnetic can be in the transient ferromagnetic-like state with parallel oriented sublattice magnetizations [15]. Such the transient magnetic state is observed in the ferrimagnetic nanolayer $Gd_{25}Fe_{65.6}Co_{9.4}$, as it is visible from measurement results of the magnetization dynamics for m_{RE} and m_{TM}, based on the method of X-ray magnetic circular dichroism (XMCD), represented in Figure 11 and Figure 12 [15].

Under the action of the laser-induced thermal pulses temperature of the ferrimagnetic nanolayer passes across the magnetization compensation temperature T_M, the sublattices Gd and FeCo switch and a new magnetization configuration m_{RE} and m_{TM} becomes by the mirror image to their initial configuration (Figure 11). Correspondingly, hysteresis loops also pass in their mirror images, as it is visible in Figure 11 (a). The magnetization dynamics of the ferrimagnetic sublattices is characterized by distinct times of the laser-induced thermal demagnetization because of the distinct atomic structure of Gd and Fe. At the process of the laser-induced remagnetization the thermal demagnetization of the sublattice RE (when $m_{RE} = 0$) occurs in some time t_{RE} that is early than the time t_{TM} of the thermal demagnetization of the sublattice TM (when $m_{TM} = 0$). The time interval $t_{RE} \le t \le t_{TM}$ corresponds to the reverse of the magnetization m_{RE} into the transient ferromagnetic-like state with the magnetization which is parallel to the magnetization m_{TM} of the sublattice TM. Such independent magnetization dynamics is related to the strong laser-induced perturbation of the exchange interaction between the ferromagnetic sublattices.

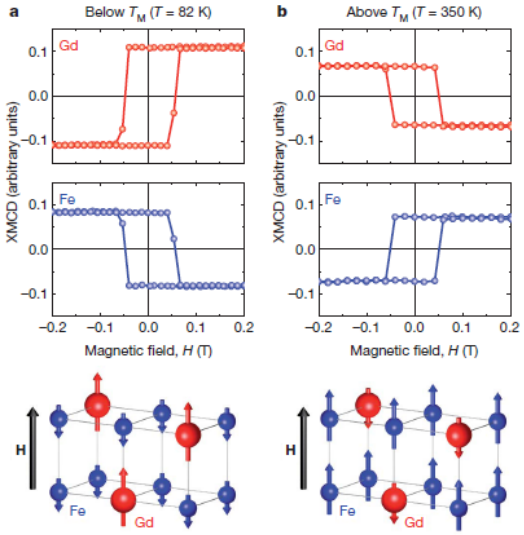

Figure 11. Ferrimagnetic alignment of the Fe and Gd magnetic moments as measured by element-specific XMCD hysteresis. a, b, Top, XMCD signals measured at the Fe and Gd absorption edges as a function of applied magnetic field below (a) and above (b) the magnetization compensation temperature (TM), demonstrating the ferrimagnetic alignment of the Fe and Gd magnetic moments. a, b, Bottom, a generic ferrimagnet, showing the alignment of the magnetic moments of the constituent sublattices with respect to the external magnetic field, H

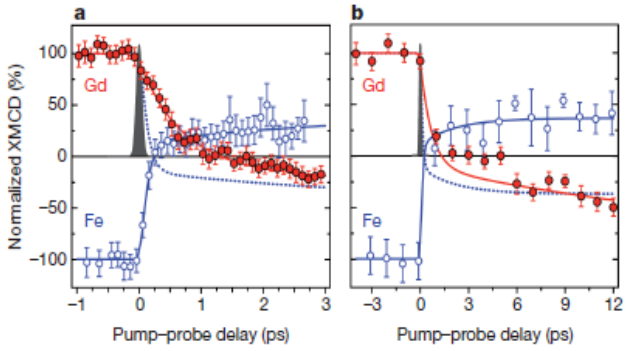

Figure 12. Element-resolved dynamics of the Fe and Gd magnetic moments measured by time-resolved XMCD with femtosecond time-resolution

Beginning with the time t_{TM} the relaxation of the antiferromagnetic exchange interaction between sublattices RE and TM results in the reverse of the magnetization m_{TM} , as it is visible in Figure 12. Beginning with the time t_{TM} the relaxation of the antiferromagnetic exchange interaction between sublattices RE and TM results in the reverse of the magnetization m_{TM} .

3.3. The Laser-Induced Thermal Remagneti-Zation of Ferrimagnetic Nanolayer

The magnetization dynamics of the ferrimagnetic under the laser-induced thermal pulses depends on the relation between the initial temperature T_{room} and the magnetization compensation temperature T_M . At $T_{room} < T_M$ the remagnetization includes the thermal demagnetization of the ferrimagnetic sublattices with subsequent transition of the magnetic state across the temperature T_M . Then remagnetization activation assumes a presence of the applied magnetic field.

At $T_{room} < T_M$ the laser-induced thermal magnetization, dynamics retains the character properties of the passage across the transient ferromagnetic-like state and the relaxation of the antiferromagnetic exchange interaction between the ferrimagnetic sublattices. In the time interval $[t_1, t_2]$ between the time points t_1 and t_2 of the thermal demagnetization of the ferrimagnetic sublattices 1 and 2 the magnetic bias of the sublattice 1 occurs in the ferrimagnetic-like exchange field of the sublattice 2 that corresponds to the transient ferromagnetic-like state. In the time point t_2 the sublattice 2 undergoes of the effective magnetic bias of the antiferromagnetic exchange interaction on the side of the sublattice 1 because of the relaxation of the antiferromagnetic exchange interaction between the sublattices. Thus, at the initial temperatures above the magnetization compensation temperature, the remagnetization of ferrimagnetic layer can occurs only under the laser-induced thermal pulses without applied magnetic fields [17]. Such the laser-induced thermal remagnetization mechanism can be described in the modified Landau-Lifshitz model [17] (Figure 13).

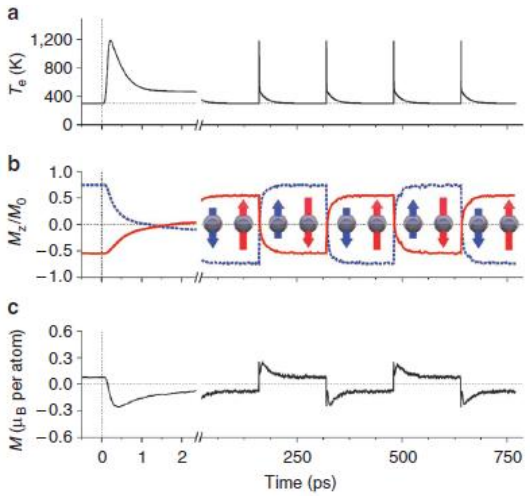

Figure 13. Computed ultrafast thermally induced switching dynamics. (**a**) Evolution of the temperature of the electronic thermal bath during a sequence of 5 Gaussian pulses. (**b**) Computed time-resolved dynamics of the z-component of the magnetizations of Fe and Gd sublattices; Gd is represented by the solid red line and the Fe by the dashed blue line. The net magnetization is shown in (**c**). A spike in the temporal behaviour of the total magnetization during the excitation is due to different dynamics of the magnetizations of the Fe and Gd sublattices

As it is visible in Figure 13 the remagnetization of the ferrimagnetic nanolayer accompanies every the lase-induced thermal pulse without applied magnetic fields. Impossibility to oppose the remagnetization by the external magnetic field less than 40 T [17] argues about large internal magnetic fields in the ferrimagnetic.

The laser-induced thermal remagnetization of the ferrimagnetic $Gd_{24}Fe_{66.5}Co_{9.5}$ was observed with the help of the magneto-optical spectroscopy based on the Faraday effect and with the help of the photoemission electron microscope (PEFM) employing the X-ray magnetic circular dichroism. In the last case, the magnetization reverse for each of the sublattices was observed [17].

Thus, purely lather-induced thermal remagnetization is possible for ferrimagnetic layers. Different speeds of the thermal demagnetization of the sublattices result in the transient ferromagnetic-like state mediating ultrafast reversal of antiferromagnetically coupled spins in the ferrimagnetic. In combination with the relaxation of the antiferromagnetic exchange interaction that results in the remagnetization effect without applied magnetic fields.

References

[1] Gerrits, Th., Van den Berg, H.A.M., Hohlfeld, J., Bär, L., and Rasing, Th., "Ultrafast precessional magnetization reversal by picosecond magnetic field pulse shaping," *Nature*, 418. 509-512. Aug.2002.

[2] Tudosa, I., Stamm, C., Kashuba, A.B., King, F., Siegmann, H. C., Stöhr, J., Ju, G., Lu, B. and Weller, D., "The ultimate speed of magnetic switching in granular recording media," *Nature Physics*, 428. 831-833. Apr.2004.

[3] Devolder, T., A., Suzuki, Y., Chappert, C., Crozat, P. and Yagam, K., "Temperature study of the spin-transfer switching speed from dc to 100 ps," *J. Appl. Phys.* 98 (5). 053904-053911. Sept.2005.

[4] Acremann, Y., Strachan, J., Chembrolu, V., Andrews, S., Tyliszczak, T., Katine, J., Carey, M., Clemens, B., Siegmann, H. and Stöh, J., "Time-Resplved Imaging of Spin Transfer Switching: Beyond the Macrospin Concept," *Phys. Rev*. Lett., 96 (21) , 217202-1− 217202-4. Jun.2006.

[5] Vahaplar, K., Kalashnikova, A. M., Kimel, A. V., Hinzke, D., Nowak, U., Chantrell, R., Tsukamoto, A., Itoh, A., Kirilyuk, A.,

and Rasing, T.,"Ultrafast Path for Optical Magnetization Reversal via a Strongly Nonequilibrium State," *Phys. Rev. Lett.* 103 (11). 117201-1−117201-4. Sept.2009.

[6] Stöhr, J. and Siegmann, H.C. *Magnetism: From Fundamentals to Nanoscale Dynamics*, Springer-Verlag Publisher, Berlin, 2006, 223.

[7] Keller, U., "Recent developments in compact ultrafast lasers," *Nature*, 424. 831-838. Aug.2003.

[8] Krupa, N.N., Korostil, A.M., "On laser-induced magnetoresistance effect in magnetic junctions," *International Journal of Modern Physics B*, 26 (31) 20146-1−20146-14. Dec.2012.

[9] Krupa, N.N., "Photo-driven spin transistor based on magnetic heterogeneous nanostructures," *in 5th International Conference on Nanoelectronic Functional Basis*, Kharkov University Publishers, 247-250, 2012.

[10] Bigot, J.-Y., Vomir, M., and Beaurepaire, E., "Coherent ultrafast magnetism induced by femtosecond laser pulses," *Nature Physics*, 5. 513-519. July. 2009.

[11] Korostil, A.M., "A field-controlled current in nanojunctions," *in 5th International Conference on Nanoelectronic Functional Basis*, Kharkov University Publishers, 54-57, 2012.

[12] Korostil, A.M., "Calculation of tunneling current in nanojunctions," *Modelling and information systems*, 64. 22-32. Aug.2012.

[13] Stanciu, C.D., Kimel, A.V., Hansteen, F., Tsukamoto, A., Itoh, A., Kirilyuk, A., and Rasing, T., "Ultrafast spin dynamics across compensation points in ferrimagnetic GdFeCo: The role of angular momentum compensation," *Phys. Rev. B*, 73(22). 220402-1−220402-4. June.2006.

[14] Stanciu, C.D., Hansteen, F., Kimel, A.V., Tsukamoto, A., Itoh, A., Kirilyuk, A., and Rasing, T., "Subpicosecond Magnetization Reversal across Ferrimagnetic Compensation Points," *Phys. Rev. Lett*. 99 (21). 217204-1−217204-4. Nov.2007.

[15] Radu, I., Vahaplar K., Stamm C.,et al., "Transient ferromagnetic-like state mediating ultrafast reversal of antiferromagnetically coupled spins," *Nature*, 472. 205-208. March.2011.

[16] Vahaplar, K., *Ultrafast Path for Magnetization Reversal in Ferrimagnetic GdFeCo Films*, Doctoral thesis, 2011.

[17] Ostler, T.A., Barker, J., Evans, R.F.L., et al., "Ultrafast heating as a sufficient stimulus for magnetization reversal in a ferrimagnet," *Nature Communications*, 3. 1-6. Feb. 2012.

[18] Pershan, P.S , Ziel, J.P , and Malmstrom, L.D., "Theoretical Discussion of the Inverse Faraday Effect, Raman Scattering, and Related Phenomena," *Phys. Rev*. 143(2).574-583.March.1966.

[19] Hertel, R , "Viewpoint: For faster magnetic switching – destroy and rebuild," J . *Phys.*: *Condens. Matter*., 2. 73-76. Sept.2009.

[20] Kimel, A.V., Kirilyuk, A., Hansteen, F., Pisarev, R.V., and Rasing, Th., "Nonthermal optic control of magnetism and ultrafast laser-induced spin dynamics in solids," *Phys.:Condens. Matter*., 19(4), 043201-043224 (2007).

[21] Gulyaev, Yu.V., Zil'berman, P.E., Epshtein E.M., and Elliott, R.J., Current-induced spin injection and surface torque in ferromagnetic metallic junctions," *JETP*, 100(5). 1005-1017. May.2005.

[22] Landau, L.D., Lifshitz, E.M., "On the theory of the dispersion of magnetic permeability in ferromagnet bodies," *Phys. Z. Sowjet.*, 8(1). 153-169. Jan.1935.

[23] Kaplan, J. and Kittel, J., "Exchange Frequency Electron Spin Resonance in Ferrites," *J. Chem. Phys*. 21(4). 760-761. Febr.1953.